Visual, Tactile, and Vibration-Based Terrain Analysis for Planetary Rovers[1,2]

Karl Iagnemma, Christopher Brooks, and Steven Dubowsky
Massachusetts Institute of Technology
Room 3-435A, 77 Massachusetts Avenue, Cambridge, MA, 02139 USA
617-452-3262
{kdi,cabrooks,dubowsky}@mit.edu

Abstract—Future planetary exploration missions will require rovers to perform difficult tasks in rough terrain, with limited human supervision. Knowledge of terrain physical characteristics would allow a rover to adapt its control and planning strategies to maximize its effectiveness. This paper describes recent and current work at MIT in the area of on-board terrain estimation and sensing utilizing visual, tactile, and vibrational feedback. A vision-based method for measuring wheel sinkage is described. A tactile method for on-line terrain parameter estimation is also presented. Finally, a method for terrain classification based on analysis of vibration in the rover suspension is described. It is shown through simulation and experimental results that these methods can lead to accurate and efficient understanding of a rover's physical surroundings.

TABLE OF CONTENTS

1. INTRODUCTION.....1
2. VISUAL WHEEL SINKAGE ESTIMATION.2
3. TERRAIN PARAMETER ESTIMATION.....4
4. VIBRATION-BASED CLASSIFICATION....6
5. CONCLUSIONS AND FUTURE WORK 7
REFERENCES 8

1. INTRODUCTION

Future planetary exploration missions will require rovers to perform challenging mobility tasks in rough terrain. Wheel-terrain interaction has been shown to play a critical role in rough-terrain mobility [1]. For example, a rover traveling through loose drift material has very different mobility characteristics than one traveling over hard, crusty terrain.

It would be desirable for rovers to gather on-line information about the surrounding terrain. This can be done by estimating terrain physical parameters (e.g., cohesion, internal friction angle, shear deformation modulus, etc.), estimating terrain traversability via non-parametric means, or by classifying terrain into pre-defined groups with known traversability properties. Knowledge of terrain characteristics would allow a rover to adapt its control and planning strategy to optimize its performance, such as maximizing traction or minimizing power consumption [2, 3]. Also, terrain parameter estimation can improve scientific understanding of planetary surface composition [4,5].

This paper describes recent and current work in the Field and Space Robotics Laboratory at MIT in algorithm development for terrain estimation and sensing. A vision-based method for measuring wheel sinkage is described. It has been shown that wheel sinkage is a key variable in estimating wheel-terrain interaction [1,6]. For example, a robot traversing loose sand might experience substantial wheel sinkage and poor mobility due to increased motion resistance. Conversely, a robot traversing firm clay might experience small wheel sinkage and high mobility. With knowledge of wheel sinkage, a mobile robot could modulate wheel torque to improve traction or adapt its motion plan to avoid potentially hazardous terrain. Wheel sinkage is also an important input to terrain identification and classification algorithms [4,6].

A terrain parameter estimation algorithm is presented that relies on a simplified form of classical terramechanics equations, and uses a linear-least squares estimator to compute terrain parameters in real time. The method is computationally efficient, and is thus suitable for implementation on a rover with limited on-board computational resources. Simulation and experimental results show that the algorithm can accurately and efficiently identify key terrain parameters for a variety of soil types.

Finally, a method for terrain classification based on analysis of vibration in the rover suspension is described. The algorithm uses principal component analysis-based classifier

[1] 0-7803-8155-6/04/$17.00©2004 IEEE
[2] IEEEAC paper #1121, Version 2, Updated July 29, 2003

of vibration signals to identify unique terrain types. Experimental results show that the algorithm can quickly and efficiently distinguish between distinct terrain types.

These methods can lead to accurate and efficient understanding of a rover's physical surroundings. Such techniques could enhance rover safety and mobility, through integration with control and motion planning methods.

2. VISUAL WHEEL SINKAGE ESTIMATION

The goal of the algorithm is to measure wheel sinkage in deformable terrain from a visual image. A more detailed treatment of this method is presented in [7]. Here we assume the presence of a camera mounted on the robot body, with a field of view containing the wheel. Sinkage is defined as a pair of angles from the vertical termed left and right terrain interface angles (see Figure 1). This represents a general description of wheel sinkage in uneven terrain. To determine these angles, only an annular region along the wheel rim (between r_{rim} and r_{wheel}) needs to be examined. This reduces computational requirements by eliminating much of the scene.

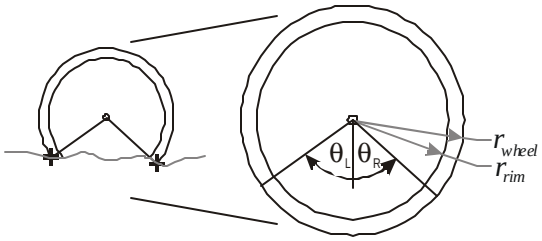

Figure 1 - Rigid wheel sinking into deformable terrain with left (θ_L) and right (θ_R) terrain interface angles shown

It is assumed that the location of the wheel relative to the camera is known. This is a reasonable assumption, since many robots have rigid suspensions. Robots with articulated suspensions (such as the Sojourner rover) are generally instrumented with suspension configuration sensors. Note that visual methods for identifying the wheel center could also be implemented.

It is also assumed that the robot wheel rim is visually distinguishable from the surrounding terrain. This is generally true for rigid, metallic wheels or dark pneumatic tires in natural terrains. Visual contrast can be enhanced by coloring the wheel rim a non soil-like color. This pixel-level difference in appearance eliminates the need for computationally-intensive texture analysis or stereo-based correlation. The algorithm instead relies on a relatively simple analysis of grayscale intensity along the wheel rim.

Algorithm Description

The algorithm consists of three steps: 1) wheel rim identification, 2) pixel intensity computation, and 3) terrain interface identification. The following sections describe these steps.

Wheel Rim Identification and Classification ¾ All points of interest on the wheel rim are first identified. Points of interest lie in a region between the inner wheel rim diameter r_{rim} and the outer wheel rim diameter r_{wheel} (see Figure 1). For rimless wheels or tires, r_{wheel} corresponds to the outer tire diameter and r_{rim} is chosen to be slightly less than r_{wheel}.

Points of interest in the annular region are divided into two regions corresponding to the left and right half of the wheel (see Figure 2). This is done since terrain entry generally occurs in one half of the wheel, and terrain exit occurs in the other. Thus the algorithm searches for one terrain interface in each region. Left and right wheel halves are determined with respect to the vector $\mathbf{v}_{down}$. The vector $\mathbf{v}_{down}$ is a unit vector perpendicular to the pitch angle of the vehicle (e.g., on flat terrain, $\mathbf{v}_{down}$ is parallel to the gravity vector).

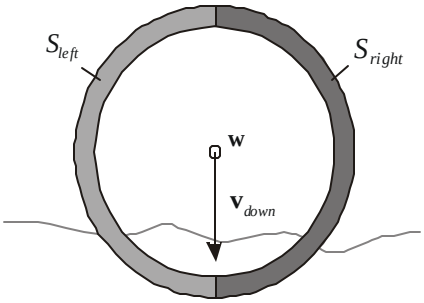

Figure 2 - Annulus sections and $\mathbf{v}_{down}$

Pixel Intensity Computation ¾ The average grayscale intensity is computed for every row of pixels in S_{right} and S_{left} (see Figure 2). A row contains multiple pixels and is perpendicular to $\mathbf{v}_{down}$. For each row the summed intensity is computed as the sum of each individual pixel's intensity. Two arrays of summed row intensities are thus formed.

Terrain Interface Identification ¾ A one-dimensional spatial Gaussian filter is employed to smooth the intensity arrays and reduce the effects of noise. Here the summed row intensities are weighted by the number of pixels in a row to minimize the influence of noise in low pixel-count rows.

A Gaussian distribution is approximated by a binomial distribution. This is applied to the summed pixel intensities to produce a pair of filtered intensity arrays. A sample plot of filtered intensity vs. angular position can be seen in Figure 3.

The location of the terrain interface is computed as the point of maximum change in intensity between rows. This exploits the fact that the wheel rim is a different color (generally brighter, for metallic wheels) than the terrain.

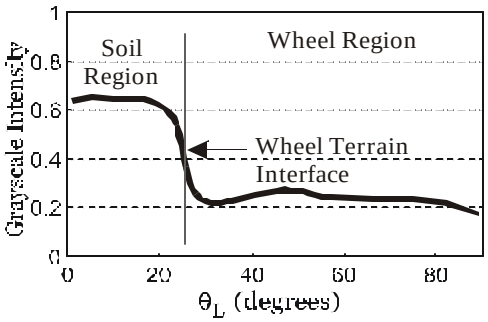

Figure 3 - Sample plot of average pixel intensity vs. angular position

Experimental Results

Experiments have been performed on the terrain characterization testbed shown in Figure 4 The testbed consists of a driven wheel mounted on an undriven vertical axis. A camera is mounted to the testbed so that it moves horizontally with the wheel, but not vertically. Images from the testbed were collected under six different terrain and lighting conditions, including variable wheel slip and terrain unevenness conditions, variable soil colors, and with and without rocks. Lighting was varied from uniform, diffuse illumination to a point-source which cast sharp shadows.

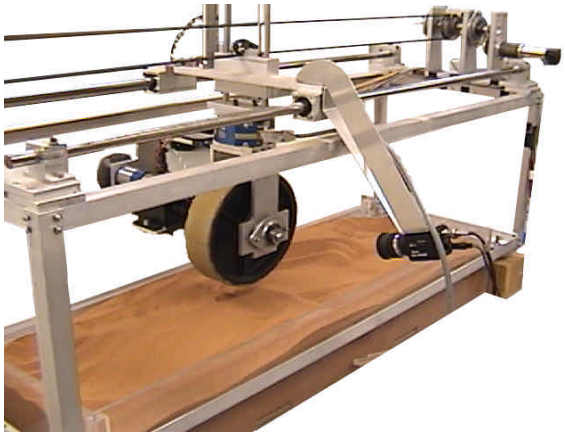

Figure 4 - Terrain characterization testbed

Representative results are shown in Figure 5. Figure 5 shows the actual and visually-measured sinkage as a percentage of the wheel radius for an image set of a wheel moving through flat, dry bentonite clay under uniform lighting, with a high slip ratio. The visually-measured sinkage matches the actual sinkage very accurately.

Over repeated trials with varying lighting conditions, the algorithm detected wheel sinkage with reasonably good accuracy. Some errors were caused by rocks occluding the wheel-terrain interface. While these small errors could be mitigated by a texture- or geometry-based rock detection algorithm, adding such an algorithm would drastically increase the computational requirements. A more significant error source was uneven lighting. Reflections off the wheel rim and shadowing on the uneven terrain led to misidentification. Note that the robot body can also cause shadowing on the wheel. However, errors due to shadowing tend to appear as easily-identifiable "outliers" (i.e., the errors are large anomalous changes in the visually-measured angle) that could be mitigated by intelligent filtering.

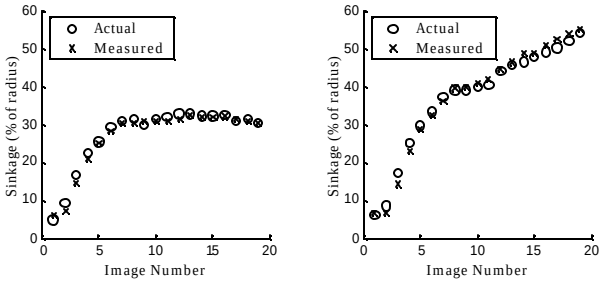

Left Side Right Side

Figure 5 - Actual and visually-measured sinkage for dried bentonite, high wheel slip, flat terrain, and diffuse lighting

An alternative method for addressing errors caused by uneven lighting is to employ active lighting. Figure 6 shows a sample image from a series where a strobe was used to illuminate the wheel-terrain interface. Here the wheel was driving through topsoil, and the wheel rim was yellow, providing good contrast. The results are plotted in Figure 7. In shadowy conditions, tests using a strobe to illuminate the wheel resulted in RMS errors less than 2% of the radius.

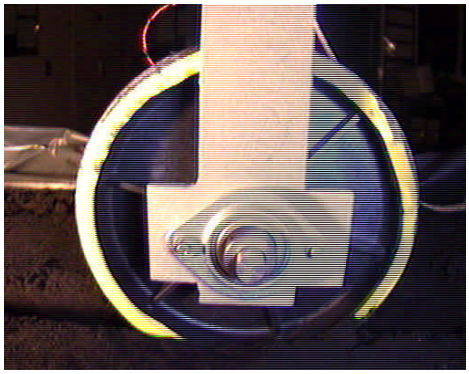

Figure 6 – Wheel traveling through topsoil with active lighting

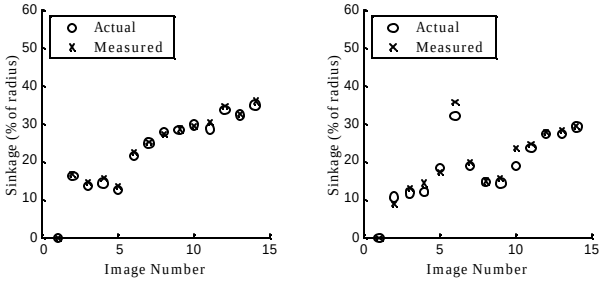

Left Side Right Side

Figure 7 - Actual and visually-measured sinkages for image set 7 (active lighting)

3. TERRAIN PARAMETER ESTIMATION

The goal of this algorithm is to estimate critical terrain parameters via "touch" (i.e., through feedback from the rover wheel, such as torque, sinkage and slip). The case of a smooth rigid wheel traveling through deformable terrain is considered, as this is the expected condition for planetary rovers. A detailed treatment of this method is given in [4]. The following analysis also applies to grousered wheels, since grousers can be modeled by an increased effective wheel radius.

To estimate terrain parameters, equations relating the parameters of interest to physically measurable quantities must be developed. The physical parameters of interest are the terrain cohesion c and the internal friction angle f. These parameters can be used to compute the maximum terrain shear strength, t_{max}, from Coulomb's equation:

$$t_{\max} = c + s_{\max} \tan f \tag{1}$$

where s_{max} is the maximum normal stress on a terrain region.

In Figure 8, a vertical load W and drawbar pull DP are applied to the wheel by the vehicle suspension. A torque T is applied at the wheel rotation axis by an actuator. The wheel has angular velocity w, and the wheel center possesses a linear velocity, V. The angle from the vertical at which the wheel first makes contact with the terrain is denoted q_1. The angle from the vertical at which the wheel loses contact with the terrain is denoted q_2. The vertical sinkage is z.

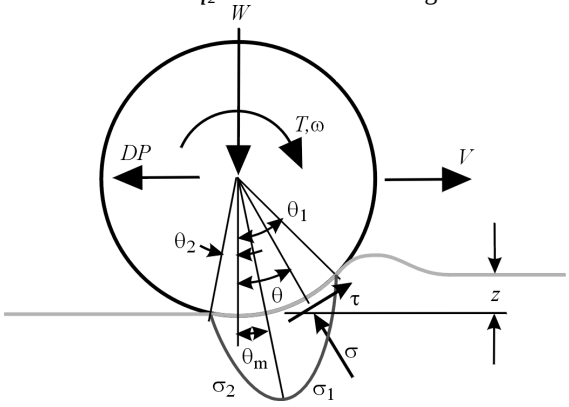

Figure 8 - Rigid wheel on deformable terrain

A stress region is created at the wheel-terrain interface, and is indicated by s_1 and s_2. The angle from the vertical at which the maximum stress occurs is denoted q_m.

From Figure 8, force balance equations can be written as:

$$W = rb\left(\int_{q_2}^{q_1} s(q)\cos q \cdot dq + \int_{q_2}^{q_1} t(q)\sin q \cdot dq\right) \tag{2}$$

$$DP = rb\left(\int_{q_2}^{q_1} t(q)\cos q \cdot dq - \int_{q_2}^{q_1} s(q)\sin q \cdot dq\right) \tag{3}$$

$$T = r^2 b\int_{q_2}^{q_1} t(q)\cdot dq \tag{4}$$

The shear stress can be computed as:

$$t(q) = \left(c + s(q)\tan f\right)\left(1 - e^{-\frac{r}{k}[q_1 - q - (1-i)(\sin q_1 - \sin q)]}\right) \tag{5}$$

where k is the shear deformation modulus, r is the wheel radius, and i is the wheel slip, defined as $i = 1 - (V/rw)$ [9].

The normal stress at the wheel-terrain interface is given by:

$$s(z) = \left(\frac{k_c}{b} + k_f\right) z^n \tag{6}$$

where b is the wheel width, k_c and k_f are pressure sinkage moduli, and n is the sinkage exponent [9].

Note that shear and normal stress are functions of c and f, among other variables. Analytical solutions of Equations (2-4) are required to obtain closed-form expressions for c and f. However, the equations' complexity motivates the use of an approximate form of the fundamental stress equations.

Figure 9 is a plot of the shear and normal stress distributions around the rim of a driven rigid wheel on various terrains. The shear and normal stress distribution curves are approximately triangular for a wide range of terrain.

Based on this observation, a linear approximation of shear and normal stress distribution equations can be written as:

$$s_1^L(q) = \frac{q_1 - q}{q_1 - q_m} s_m \tag{7}$$

$$s_2^L(q) = \frac{q}{q_m} s_m \tag{8}$$

$$t_1^L(q) = \frac{q_1 - q}{q_1 - q_m} t_m \tag{9}$$

$$t_2^L(q) = c + \frac{q}{q_m}(t_m - c) \tag{10}$$

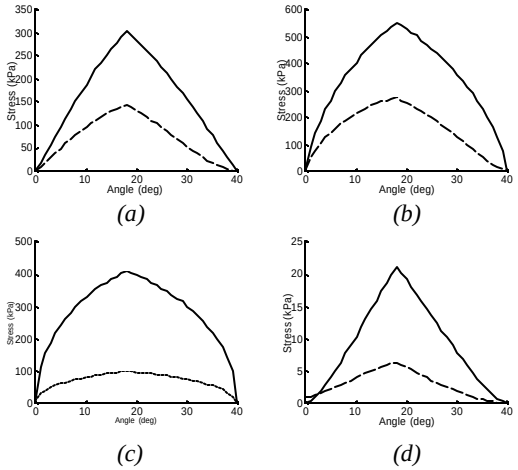

Figure 9 - Normal (solid) and shear stress (dotted) for (a) dry sand, (b) sandy loam, (c) clayey soil, and (d) snow [1, 9]

Simplified forms of the force balance equations can be written and solved for the load W and torque T:

$$W = \frac{rb}{q_m(q_1 - q_m)} \begin{bmatrix} s_m(-q_m \cos q_1 + q_1 \cos q_m - q_1 + q_m) \\ -t_m(q_m \sin q_1 - q_1 \sin q_m) \\ -c(q_1 \sin q_m - q_m \sin q_m - q_m q_1 + q_m^2) \end{bmatrix} \quad (11)$$

$$T = \frac{r^2 b}{2}(t_m q_1 + c q_m) \quad (12)$$

An additional equation can be written if the location of the maximum shear and normal stress are assumed to occur at the same location q_m:

$$t_m = (c + s_m \tan f)\left(1 - e^{-\frac{r}{k}[q_1 - q_m - (1-i)(\sin q_1 - \sin q_m)]}\right) \quad (13)$$

The simplified equations can be solved for the cohesion and internal shear angle and rearranged in the following form (after additional simplification):

$$\frac{k_2}{k_3} = c + \frac{k_1}{k_3} \tan f \quad (14)$$

where

$$k_1 = A\left(q_1^2 W r + 4T \sin q_1 - 8T \sin \frac{q_1}{2}\right)$$

$$k_2 = 4T\left(\cos q_1 - 2\cos\frac{q_1}{2} + 1\right)$$

$$k_3 = q_1 r^2 b\left(\cos q_1 - 2\cos\frac{q_1}{2} + 2A\cos q_1 - 4A\cos\frac{q_1}{2} + 2A + 1\right)$$

and $A = 1 - e^{-\frac{r}{k}\left[\frac{q_1}{2} + (1-i)\left(-\sin q_1 + \sin\left(\frac{q_1}{2}\right)\right)\right]}$.

Equation (14) is a single equation in two unknowns. At least two unique instances of Equation (14) are required to determine c and f. In practice numerous unique instances of Equation (14) can be written as a rover moves through terrain. Least-squares techniques can then be used to solve for c and f.

Figure 10 shows representative results of parameter estimation simulation for dry, sandy soil. It can be seen that the estimated parameters c and f quickly converge to the true values of c = 2.5 and f = 27.0.

Figure 11 shows experimental results of parameter estimation of dried bentonite clay performed on a wheel-terrain interaction testbed (see Figure 5). Again, it can be seen that c and f quickly approach the measured values of c = 0.7 and f = 32.1.

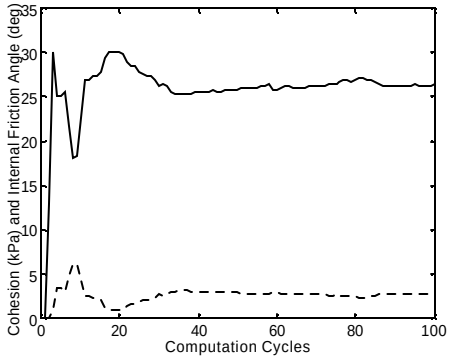

Figure 10 - Simulated estimation of cohesion (dotted) and internal friction angle (solid)

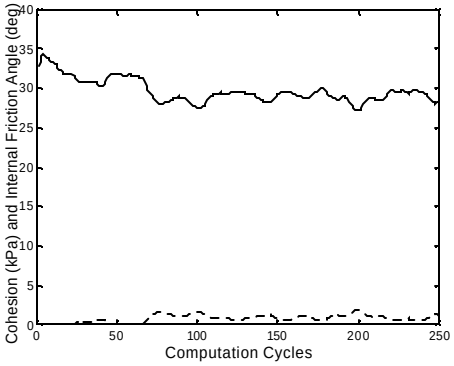

Figure 11 - Experimental estimation of cohesion (dotted) and internal friction angle (solid)

These results show that the algorithm produces accurate, on-line parameter estimates on an experimental system with noisy sensors. The algorithm takes only a few msec per estimation cycle on a desktop PC, thus making it feasible for on-board implementation on a rover with limited computational resources.

Terrain parameter estimates from this algorithm can be used to optimize a rover's mobility and safety, and are themselves useful scientific information.

4. VIBRATION-BASED TERRAIN CLASSIFICATION

The goal of this algorithm is categorize terrain that a rover is currently traversing into gross terrain classes (i.e. "sandy terrain", "rocky terrain", "mixed terrain") based on analysis of vibration signals present in the rover suspension. Empirical observation has shown that different terrain physical properties give rise to unique vibration signatures in the lightly-damped rover wheel assembly and suspension frame. Here we assume that an accelerometer or contact acoustic transducer will be used to record the high-frequency vibrations. We also assume the sampling rate is sufficiently high to capture frequencies of interest.

Algorithm Description

The algorithm relies on principal component analysis (PCA) to distinguish between terrain classes. The algorithm is composed of two steps: *a priori* analysis, and on-line classification. The following sections describe these steps. For simplicity we here present the case where a rover attempts to classify two distinct terrain types.

A priori analysis¾A priori experiments are performed with terrain classes that grossly correspond to classes the rover would like to identify on-line. For example, *a priori* experiments might be performed with sandy terrain and crusty terrain.

For a given terrain pair, raw vibration data is collected. This data is divided into short segments for which the log power spectral density is estimated. Matrices $\mathbf{Y}_{\text{sand}}$ and $\mathbf{Y}_{\text{gravel}}$ are summaries of the data, with each column containing the spectral content for a given segment and each row showing the variation in spectral content at a given frequency as a function of time:

$$\mathbf{Y}_{sand} = \begin{bmatrix} y_{sand,\,fmin,t=1} & \cdots & y_{sand,\,fmin,t=n} \\ \vdots & \ddots & \vdots \\ y_{sand,\,fmax,t=1} & \cdots & y_{sand,\,fmax,t=n} \end{bmatrix}. \qquad (15)$$

The two datasets are then combined, $\mathbf{Y} = [\mathbf{Y}_{sand} \quad \mathbf{Y}_{gravel}]$ ($\mathbf{Y} \in \Re^{m \times n}$), and the rows are mean-adjusted to form the matrix $\hat{\mathbf{Y}}$:

$$\overline{\mathbf{Y}} = \begin{bmatrix} mean(y_{fmin}) \\ \vdots \\ mean(y_{fmax}) \end{bmatrix} [1 \quad \cdots \quad 1] \qquad (16)$$

$$\hat{\mathbf{Y}} = \mathbf{Y} - \overline{\mathbf{Y}} \qquad (17)$$

Singular value decomposition is used to separate $\hat{\mathbf{Y}}$ into three matrices, $\mathbf{U}_a$, $\mathbf{S}_a$, and $\mathbf{V}_a$:

$$\hat{\mathbf{Y}} \xrightarrow{SVD} (\mathbf{U}_a, \mathbf{S}_a, \mathbf{V}_a')$$

Here, $\mathbf{U}_a$ and $\mathbf{V}_a$ are unitary matrices and $\mathbf{S}_a$ is a diagonal matrix of singular values. The matrix $\mathbf{U}_a$ is assumed to be composed of orthogonal signal and noise subspaces. For signal representation we extract k principal components corresponding to the signal space to create the matrix $\mathbf{U}_{\text{signal}}$. In practice we have used k=6, as it appears to give good signal representation without overfitting. Similarly, the first k rows and columns of $\mathbf{S}$ will be referred to as $\mathbf{S}_{\mathbf{signal}}$. These two matrices can be considered to be a map from the full frequency space ($\mathbf{R}^m$) to the signal space ($\mathbf{R}^k$). The signal space mappings of the separate datasets $\mathbf{Y}_{\text{sand}}$ and $\mathbf{Y}_{\text{gravel}}$ are computed as:

$$\mathbf{V}'_{sand} = \mathbf{S}_{signal}^{-1} \mathbf{U}'_{signal} \mathbf{Y}_{sand} \qquad (18)$$

$$\mathbf{V}'_{gravel} = \mathbf{S}_{signal}^{-1} \mathbf{U}'_{signal} \mathbf{Y}_{gravel} \qquad (19)$$

In this representation the columns of $\mathbf{V}'_{sand}$ and $\mathbf{V}'_{gravel}$ still correspond to a time segment, and the rows correspond to a principal component. Taking each column as a vector in a k-dimensional space, $\mathbf{V}'_{sand}$ and $\mathbf{V}'_{gravel}$ represent point-clouds centered on $\overline{\mathbf{v}}'_{sand}$ and $\overline{\mathbf{v}}'_{gravel}$ respectively.

One candidate discrimination metric for an arbitrary vector $\mathbf{v}'$ in this space would be the dot product of $\mathbf{v}'$ with the difference between $\overline{\mathbf{v}}'_{sand}$ and $\overline{\mathbf{v}}'_{gravel}$. This rarely yields satisfactory results, however, because the distributions of $\mathbf{V}'_{sand}$ and $\mathbf{V}'_{gravel}$ may have vastly different scales in the different dimensions.

To determine a more appropriate scaling of the space, it is important to examine the separation of the points within a class, rather than between classes. This is accomplished by performing a second singular value decomposition, this time on a matrix $\hat{\mathbf{V}}'$, formed by merging mean-adjusted matrices $\hat{\mathbf{V}}'_{sand}$ and $\hat{\mathbf{V}}'_{gravel}$:

$$\hat{\mathbf{V}}'_{sand} = \mathbf{V}'_{sand} - \overline{\mathbf{v}}'_{sand} [1 \quad \cdots \quad 1] \qquad (20)$$

$$\hat{\mathbf{V}}'_{gravel} = \mathbf{V}'_{gravel} - \overline{\mathbf{v}}'_{gravel} [1 \quad \cdots \quad 1] \qquad (21)$$

$$\hat{\mathbf{V}}' = \left[\hat{\mathbf{V}}'_{sand} \quad \hat{\mathbf{V}}'_{gravel}\right] \qquad (22)$$

$$\hat{\mathbf{V}}' \xrightarrow{SVD} (\mathbf{U}_b, \mathbf{S}_b, \mathbf{V}'_b).$$

$\mathbf{V}'_b$ has columns associated with a given segment, and rows associated with a combination of the principal components. More importantly, the norm of each of the rows of $\mathbf{V}'_b$ is 1, meaning that the standard deviations of the combined intra-set distributions is equal for all of the dimensions. This scaling of the principal component space is appropriate for classifying data.

Our discrimination metric is therefore a dot product of a vector of test data $\mathbf{y}_{\text{test}}$ with the difference of class means ($\overline{\mathbf{v}}'_{sand} - \overline{\mathbf{v}}'_{gravel}$) in this scaled space. Putting all of these transformations together, we arrive at the final discrimination metric to distinguish between sandy terrain and gravel:

$$d(\mathbf{y}_{test}) = \left((\overline{\mathbf{v}}'_{gravel} - \overline{\mathbf{v}}'_{sand})' \mathbf{U}_b (\mathbf{S}_b^{-1})' \mathbf{S}_b^{-1} \mathbf{U}'_b \mathbf{S}_{signal}^{-1} \mathbf{U}'_{signal} \right) \mathbf{y}_{test} \qquad (23)$$

This is the linear combination of frequencies which best discriminates between the two datasets.

*On-Line classification¾*The *a priori* analysis results in a scalar metric for each terrain class of interest. In practice, multiple training sets would be collected under varying conditions (wheel slip, wheel load, wheel velocity) for the same terrain class. A mean and standard deviation of the discrimination metric would be collected for each class and stored on-line.

During rover traverse, a discrimination metric is computed in real-time. Terrain is classified as belonging to a class (1 or 2) if it falls within the band defined by the discrimination metric mean plus and minus one standard deviation. If the metric

does not fall within either band, the terrain is classified as unknown.

Experimental Results

Experiments have been performed on the terrain characterization testbed shown in Figure 4, here equipped with an inexpensive contact acoustic transducer mounted to the wheel assembly. Loose gravel and the Mars soil simulant JSC Mars-1 were the terrain classes of interest [10]. Physically, the gravel was composed of 1-2 cm diameter irregularly shaped stones, while the JSC Mars-1 contained a range of particle sizes ranging from fine sand to 1-2 cm rocks.

A priori training data was collected for each set over varying wheel slip, wheel sinkage, and wheel speed. Discrimination tests were performed using the leave-one-out method for training the algorithm.

Preliminary results show that the algorithm can construct a reliable scalar metric for discriminating between the loose gravel and Mars-1 soil simulant. A sample set of training data is shown in Figures 12 and 13. From Figure 12 it is clear that there is a large region of confusion between the two terrain types if the first two principal components are used for discrimination. Figure 13 shows the same data, but with the discrimination metric along the x-axis. A simple threshold of this discrimination metric correctly classifies almost all of the training data.

In Figure 14, the discrimination metric is applied to an untrained data set containing a transition from gravel to Mars-1 soil. The transition from one terrain type to the other is easy to detect.

These results suggest that vibration-based terrain sensing has much promise for quick, efficient, and robust classification of terrain.

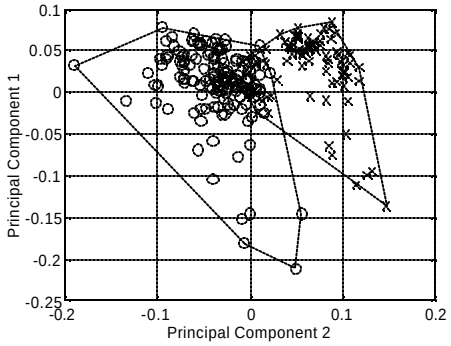

Figure 12 - Gravel and JSC Mars-1 plotted in the first two principal components

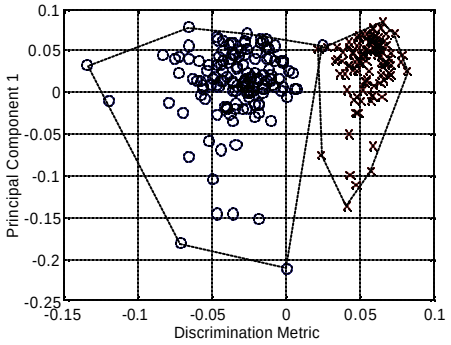

Figure 13 - Gravel and JSC Mars-1 plotted with the proposed discrimination metric along the x-axis

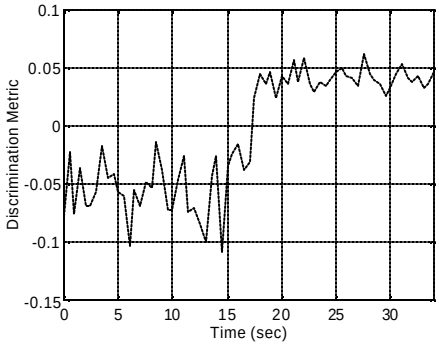

Figure 14 - Time series of discrimination metric over an untrained transition from gravel to JSC Mars-1

5. CONCLUSIONS AND FUTURE WORK

This paper has presented methods for terrain estimation and sensing. A vision-based method for measuring wheel sinkage was described and shown to be accurate and relatively robust to lighting variation. A method for on-line terrain parameter estimation was presented and shown to be effective in simulation and experimental trials. Finally, a methods for vibration-based classification of terrain type was presented and experimentally validated for several different terrain types. It was shown that these techniques can be used to gain important information about a rover's surrounding terrain.

Future work in this area will focus on intelligently integrating multiple sensing modalities to improve terrain characterization.

ACKNOWLEDGMENTS

This work is currently supported by the NASA Jet Propulsion Laboratory through the Mars Technology Program. The authors would like to acknowledge the support of Drs. Paul Schenker, Samad Hayati, and Rich Volpe.

REFERENCES

[1] G. Bekker, *Introduction to Terrain-Vehicle Systems*, University of Michigan Press, 1969.

[2] K. Iagnemma, F. Genot and S. Dubowsky, "Rapid Physics-based Rough-Terrain Rover Planning with Sensor and Control Uncertainty", *Proc. of the IEEE International conference on Robotics & Automation*, 1999.

[3] K. Iagnemma, and S. Dubowsky, "Mobile Robot Rough-Terrain Control (RTC) for Planetary Exploration," *Proceedings of the 26th ASME Biennial Mechanisms and Robotics Conference, DETC 2000*, 2000.

[4] K. Iagnemma, H. Shibly, and S. Dubowsky, "On-Line Terrain Parameter Estimation for Planetary Rovers," *Proc. of IEEE International Conference on Robotics and Automation*, 2002

[5] J. Matijevic, *et al*., "Characterization of Martian Surface Deposits by the Mars Pathfinder Rover, Sojourner," *Science*, **278**, 5, 1997

[6] S. Kang, *Terrain Parameter Estimation and Traversability Assessment for Mobile Robots*, Master's Thesis, Department of Mechanical Engineering, MIT, 2003

[7] C. Brooks, K. Iagnemma, and S. Dubowsky, "Visual Wheel Sinkage Measurement for Mobile Robot Mobility Characterization," Submitted to the *IEEE Transactions on Robotics and Automation*

[9] J. Wong, *Theory of Ground Vehicles*, Wiley, 2001.

[10] C. Allen, R. Morris, K. Jager, D. Golden, D. Lindstrom, M. Lindstrom, and J. Lockwood, "Martian Regolith Simulant JSC Mars-1," *Proceedings of the Lunar and Planetary Science Conference XXIX*, 1998

BIOGRAPHY

Karl Iagnemma *is a research scientist in the Mechanical Engineering department of the Massachusetts Institute of Technology. He received his B.S. degree summa cum laude in mechanical engineering from the University of Michigan in 1994, and his M.S. and Ph.D. from the Massachusetts Institute of Technology, where he was a National Science Foundation graduate fellow, in 1997 and 2001, respectively. He has been a visiting researcher at the Jet Propulsion Laboratory. His research interests include rough-terrain mobile robot control and motion planning, robot-terrain interaction, and robotic mobility analysis. He is a member of IEEE and Sigma Xi.*

Christopher Brooks *is a M.S. candidate in the Mechanical Engineering department of the Massachusetts Institute of Technology. He received his B.S. degree with honor in engineering and applied science from the California Institute of Technology in 2000. Prior to beginning his graduate studies, he was a manufacturing engineer at a Corning optical fiber plant. His current research interests include terrain sensing for mobile robots and machine learning. He is a member of Tau Beta Pi.*

Steven Dubowsky *received his Bachelor's degree from Rensselaer Polytechnic Institute of Troy, New York in 1963, and his M.S and Sc.D. degrees from Columbia, University in 1964 and 1971. He is currently a Professor of Mechanical Engineering at M.I.T. He has been a Professor of Engineering and Applied Science at the University of California, Los Angeles, a Visiting Professor at Cambridge University, Cambridge, England, and Visiting Professor at the California Institute of Technology, University of Paris (VI), and Stanford. During the period from 1963 to 1971, he was employed by the Perkin-Elmer Corporation, the General Dynamics Corporation, and the American Electric Power Service Corporation. Dr. Dubowsky's research has included the development of modeling techniques for manipulator flexibility and the development of optimal and self-learning adaptive control procedures for rigid and flexible robotic manipulators. He has also made important contributions to the areas of field and space robotics. He has authored or coauthored nearly 100 papers in the area of the dynamics, control and design of high performance mechanical, electromechanical, and robotic systems. Professor Dubowsky is a registered Professional Engineer in the State of California and has served as an advisor to the National Science Foundation, the National Academy of Science/Engineering, the Department of Energy, the U.S. Army and industry. He has been elected a fellow of the ASME and IEEE. He is a member of Sigma Xi and Tau Beta Pi.*